Quantitative phase imaging of cells using White Light Diffraction Phase Microscopy

Kalva Sandeep Kumar

A Dissertation Submitted to
Indian Institute of Technology Hyderabad
In Partial Fulfillment of the Requirements for
The Degree of Master of Technology

भारतीय प्रौद्योगिकी संस्थान हैदराबाद
Indian Institute of Technology Hyderabad

Department of Biomedical Engineering

June, 2015

Declaration

I declare that this written submission represents my ideas in my own words, and where others' ideas or words have been included, I have adequately cited and referenced the original sources. I also declare that I have adhered to all principles of academic honesty and integrity and have not misrepresented or fabricated or falsified any idea/data/fact/source in my submission. I understand that any violation of the above will be a cause for disciplinary action by the Institute and can also evoke penal action from the sources that have thus not been properly cited, or from whom proper permission has not been taken when needed.

(Signature)

Kalva Sandeep Kumar
(– Student Name –)

BM13M1002 .
(Roll No)

Approval Sheet

This thesis entitled "Quantitative phase imaging of cells using white light diffraction phase microscopy" Kalva Sandeep Kumar is approved for the degree of Master of Technology from IIT Hyderabad.

Dr. Harikrishnan. N. Unni
Internal Examiner

Dr. Renu John
Associate Professor and Head
Department of Biomedical Engineering
Indian Institute of Technology, Hyderabad

Vandana Sharma
(Dr. V. Sharma,
Phy. Dept.)

Acknowledgements

Dedicated to

My parents.

Abstract

Quantitative phase imaging (QPI) techniques are very advantageous compared to the qualitative phase imaging techniques like bright field microscopy, phase contrast microscopy, differential interference contrast microscopy as the QPI techniques render phase information quantitatively whereas qualitative phase imaging techniques yield phase information qualitatively and cannot provide exact phase values. In QPI techniques, there is no need of exogenous contrast agents to stain or tag the specimen. White light diffraction phase microscopy (wDPM) is one of the QPI techniques which is used to quantify the phase information from the samples. The phase information retrieved is dependent on the local refractive index and thickness of the biological cells. So, by knowing the phase we can know the index and thickness of the specimen in nanometer scales. In this technique, due to its single shot feature the acquisition speed is only limited by the sensing device, it is better compared to other quantitative phase imaging techniques as its common path geometry provides better temporal phase sensitivity by cancelling out the most mechanisms responsible for noise and with the use of white light source the images are speckle-free. So we achieve better spatial phase sensitivity compared to other techniques. This method has attractive applications in biomedicine. We have developed wDPM set up for extracting phase information from the live yeast cells and sperm cells. A fast phase reconstruction algorithm has been used to reconstruct the phase from the recorded interferograms. This algorithm avoids the unwrapping step which is needed in conventional phase reconstruction by Hilbert's transform method. We have calculated the thickness of the yeast cells and sperm cells and recorded a video for visualizing the dynamics of yeast cells.

Abbreviations

CT	Computed Tomography
MRI	Magnetic Resonance Imaging
PET	Positron Emission Tomography
SPECT	Single Photon Emission Computed Tomography
FDG	Fluorodeoxyglucose
MSA	Microscopy Society of America
TEM	Transmission Electron Microscope
SEM	Scanning Electron Microscope
STM	Scanning Tunneling Microscope
AFM	Atomic Force Microscope
SPM	Scanning Probe Microscopy
MO	Microscopic Objective
NA	Numerical Aperture
GFP	Green Fluorescent Protein
DIC	Differential Interference Contrast Microscopy
QPI	Quantitative Phase Imaging
DHM	Digital Holographic Microscopy
HPM	Hilbert Phase Microscopy
OQM	Optical Quadrature Microscopy
FPM	Fourier Phase Microscopy
DPM	Diffraction Phase Microscopy
SLIM	Spatial Light Interference Microscopy
iSLIM	Instantaneous Spatial Light Interference Microscopy
TIE	Transport of Intensity Equation
wDPM	White Light Diffraction Phase Microscopy
FOV	Field Of View
CCD	Charged Couple Devices

List of Figures

List of Tables

Contents

Chapter 1

Introduction

1.1   Bio-medical imaging

Medical imaging is a technique of representing visually the internal structures for diagnosing and treating the diseases. There are various imaging modalities for yielding the images of internal details of the body in non-invasive fashion. X-ray imaging was the earliest imaging modality used for observing the anatomical structures of the body after the discovery of X-rays by Wilhelm Rontgen in 1895. X-ray machines are still in use by the hospitals for visualizing and diagnosing the abnormalities though the X-rays exposure induces cancer if exposed repeatedly or for a long time. In late 1940's, ultrasound imaging modality has started. Ultrasound uses acoustic waves for imaging. In 1950's, first positron imaging device was developed to localize tumor inside brain. Later the device was extended to topographic mode. Computed tomography (CT) was invented by Godfrey Hounsfield. CT uses X-rays to produce tomographic images of scanned object non-invasively. Paul Lauterbur and Peter Mansfield [1] independently published an invaluable clinical and research tool, Magnetic resonance imaging (MRI) in 1974. MRI uses a strong magnetic field as a probe for imaging. Positron emission tomography (PET) uses the principle of positron emission for imaging. Single-photon emission computed tomography (SPECT) is a nuclear medicine tomographic imaging technique that uses gamma rays. These different imaging modalities use different energy sources for imaging. Multimodality imaging techniques like PET-CT, PET-MRI, CT-MRI came into existence later on that helps to extract more information about the patient.

1.1.1   Applications of bio-medical imaging

The medical imaging technologies are mainly helpful for diagnosing and treatment of diseases. X-ray imaging depicts the abnormalities in bone structures like bone fractures, displacements of bones, and information about kidney stones, gall stones and the position of metallic implants inside the body. Digital x-ray imaging is very useful in medical research,

pharmacy and pathology. Ultrasound has notable applications in obstetrics, cardiology, gynecology, surgery, pediatrics, radiology and neurology [2]. The weight and size of the baby can be estimated using ultrasound imaging. Ultrasound is also used to diagnose heart by measuring blood flow. Positron emission tomography has many applications in medical field. It is used for in-vivo examination of brain functions [3]. PET is useful for quantification of cerebral blood flow, metabolism and receptor binding. The main radiotracer in clinical use is F-18 fluorodeoxyglucose (FDG) which is majorly helpful in cardiac and neurological applications as well as in oncology [4]. FDG-PET is used for diagnosis and assessing response cancer therapy. It has many applications in cardiology like assessment of myocardial blood flow, evaluation of beta receptors in heart, used to quantify the extent of heart disease. Computed tomography (CT) has many clinical applications that include CT angiography, cardiac scoring, evaluation of brain perfusion, evaluation of acute chest pain or dyspnea, virtual endoscopy, CT myelography and in musculoskeletal applications [5]. MRI is used for a huge range of clinical applications. In clinical neurology, it is used for segmentation and classification, measuring volumes of brain structures, multiple sclerosis, neurodegeneracy and to detect strokes. MRI has applications in cardiology for fast imaging in harmony with the heart motion. With the help of MRI, we can detect breast, colorectal, liver, prostate cancers. We can also detect any damages to soft tissues like cartilage, ligaments etc. MRI is used in great deal to study brain function and cancer growth [6].

1.2   Optical imaging

Optical imaging allows for non-invasively looking inside the body and has a number of advantages compared to radiological imaging techniques. Optical imaging is used for particularly observing the soft tissues. Optical imaging of biological cells depends on how well the light interacts with the cell. All the biological living cells are transparent. When the light falls on specimen, either of the absorption, scattering, diffraction and interference phenomenon occurs. Based on the properties of the tissue, the interaction is dependent. With the help of optical imaging, structures across wide range of sizes and types can be imaged. It can be combined with other imaging modalities like MRI, X-rays etc. to provide enhanced information to doctors for monitoring complex diseases. Usage of non-ionizing radiation like visible, ultrasound and infrared light in optical imaging techniques, reduces patient's exposure to harmful radiation. This is much safer for patients and significantly has faster image acquisition rates. Therefore, it can be used for repeated procedures to monitor the progression of the diseases or to test the results of the treatment given to the patient. Optical imaging techniques has lot of in vitro and ex vivo applications in molecular and cellular biology.

Appreciable change in optical molecular imaging techniques observed due to the development of targeted bioluminescence probes, near-infrared fluorochromes and red-shifted fluorescent proteins [7]. Optical techniques have the advantage of using multiple probes for multichannel imaging. Study of gene expression in animal models can be done using optical imaging.

1.3   Microscope

Microscopy Society of America (MSA) refers microscopy as "the study of objects that are too small to be viewed by the unaided human eye. Viewing object that range in size from millimeters to nanometers has always been fascinating to people from all walks of life, and is currently also applicable to virtually every field of science and technology". A microscope is an instrument that is designed to magnify small objects. It accomplishes three tasks: produces the magnified image of the object, separates the details in the image and makes the details visible to the human eye or camera. Microscope uses various types of illumination sources like light, electrons, ions, x-rays and even mechanical probes to render images. Human eye can perceive the light only in visible spectrum. We cannot perceive outside this range (for instance, ultraviolet and infrared rays). It is sensitive to the intensity changes but not the phase property of light. With the help of different microscopy techniques, we can know all the parameters of light reflected by the object. The real image formed by the microscope can be either seen with human eye or recorded using CCD, whereas, the virtual images can only be seen and cannot be recorded.

Based on the interaction with the sample to generate image, microscopes are broadly categorized into three types:

1. Optical microscope,
2. Electron microscope,
3. Scanning probe microscope

Optical microscope magnifies the image using lenses and uses light source to illuminate the object. An optical microscopy can be either a transmission microscopy or reflection microscopy depending on the object .The interaction of the light with the sample can be absorption, scattering and fluorescence. The final image formation depends on the type of interaction. Absorption of light by the specimen depends on the wavelength of the light and the type of tissue. Beer-lamberts law states the relationship between intensity of light and absorption coefficient with penetration depth as follows:

$$\mathbf{I = I_0 e^{-\mu_a z}} \tag{1.1}$$

3

where I_0 is initial intensity of light, μ_a is the absorption coefficient and Z is the penetration depth. Absorption coefficient shows how intensity of light changes as light penetrates through the tissue. So, the light after passing the object varies in intensity depending upon the absorption coefficient, this reduced intensity light gives information about the object. Bright field microscopy is one of the optical microscopic technique that is based on the absorption coefficient of the biological specimen. Biological cells are weak in absorption, therefore they cannot be images with better contrast using bright field microscopy. Biological tissues are highly or weakly scattering. Detection of bacterial cells by light scattering methods is explained by Billy et.al [8]. Dark field microscope produces images with dark background and contrast appears because of the scattering of light from the sample. When the sample is illuminated with the band of light, light of particular wavelength is absorbed and light of different wavelength is emitted by the sample. This property is termed as fluorescence and microscope used is fluorescence microscopy. Apart from the absorption, scattering and fluorescence, phase property of light can be used for imaging as in phase contrast microscopy and differential interference contrast microscopy. Polarization of light also helps in imaging the biological specimen as in polarizing light microscopy, DIC also uses polarization property of light. Stereo microscope is also one of the optical microscopic techniques that produces three dimensional visualization of the sample. It has two separate paths with two eyepieces and two objectives to provide different viewing angles of the same sample at a time.

Electron microscope uses a beam of accelerated electrons as source of illumination. The first apparatus of electron microscopy took its shape in 1931 by German physicist Ernst Ruska and electrical engineer Max Knoll. The resolving power is higher for electron microscopes and has magnification factor compared to optical microscopes. The greater resolution is because of the smaller wavelength of the electron compared to optical wavelengths. The transmission electron microscope (TEM) is the original form of electron microscope that uses a high voltage electron beam to create an image. Siemens developed first commercial TEM in 1939 [9]. Scanning electron microscope (SEM) scan the sample surface where electron interacts with the surface of the sample, contains topographical information of the surface composition and electrical conductivity. Because of its high resolving nature, electron microscope has various biological applications. With the help of electron microscope, the internal structures and organelles of cells can be clearly seen. Some of the disadvantages of using electron microscope are, the equipment is very expensive to build and maintain, sample preparation involves difficult procedures and consumes lot of time. In addition to that samples must be

dry and should be fixed for imaging. This implies live cell imaging is not feasible with electron microscope. The energy of electron beam is so high that it may harm the biological sample. Thus, optical microscope is best suitable for live cell imaging compared to electron microscope though resolution and magnification are limited in optical microscope. The current research using optical microscopes is much focused on the improvisation of resolution and contrast for enhanced understanding of live cells.

Scanning probe microscopy forms images of surfaces using a probe that scans the specimen. Gerd Binnig and Heinrich Rohrer in 1981 invented the scanning tunneling microscope (STM). Later in 1986, Gerd Binni, Quate and Gerber invented atomic force microscope (AFM).The microscopic images are formed by the interaction of the tip of the cantilever beam with surface of the sample. Based on this interaction computer gathers information about the image. The interaction between the tip of cantilever and sample can be mechanical force, electrostatic force, chemical interaction, Vander walls forces or capillary forces. AFM is used to detect the cell morphology and topology and to find the surface details of the structural proteins [10]. Resolution is high for SPM compared to optical microscope. But the SPM takes long time for scanning and imaging the cells and they may damage the cells while scanning and it is not useful for lateral imaging.

So, the three microscopic techniques have myriad of biological applications and each one has its own advantages and disadvantages. Live cell imaging is the current research wherein the researchers are trying to obtain the nanoscale variations of different parameters of the cell and cell organelles. The imaging environment should be as similar as to the in situ environment of the specimen so that there won't be any disturbance for the sequential metabolic processes that takes place inside the cell. Hence, live cell imaging is a big challenge. Using electron microscope, though we achieve highly resolution images of cells, the electron radiation damages the cells resulting in altered images of the actual live cells. Scanning probe microscopy (SPM) also renders better resolution to the nanometer scales but live cell imaging is not possible and the time for scanning the cells is also high and some of the SPM techniques may damage the cells.

Optical microscopic techniques are preferable for live cell imaging as it doesn't damage any cell, thus renders images of intact live cells. Optical techniques are non-invasive and non-destructive. These use light which is radiation free resulting in no damage the specimen and

5

can form images of different colors because of the visible spectrum and colors are seen to as result of staining. These actually doesn't require staining unless we need more contrast in the sample.

1.4   Basic concepts in optical microscopy

Modern compound optical microscopes utilizes dual stage magnifying design that includes primary imaging lens, *objective*, coupled to secondary visualizing lens system, *eye piece* or *ocular* mounted at opposite ends of the tube. Basics concepts necessary for complete understanding of microscopy includes objectives, magnification, numerical aperture, resolution, optical aberrations.

1.4.1   Microscope Objectives

Microscope objective (MO) is the most important component in optical microscope that focuses the light originating from the specimen. It forms the primary image which is then subsequently magnified by eye piece. MO is selected for particular application based on numerical aperture (NA) as NA decides the resolution. The magnification of MO is selected such that the specimen can be seen clearly. Figure 1.1 gives an idea about MO.
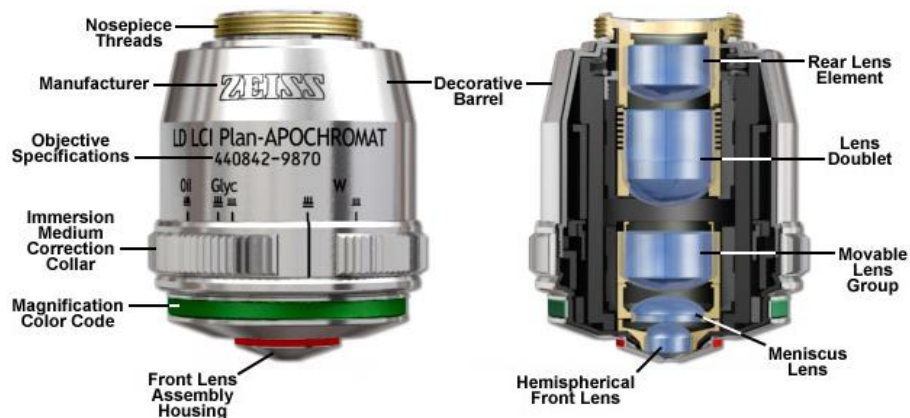
Figure 1-1: Microscope objective anatomy and specifications [11]

MO is placed very close to the specimen in the set up that collects maximum rays diffracted from the sample. It is the first component that light encounters as it passes from specimen to image plane. MO is the most difficult component to design and assemble as it is a combination of many micro-lenses. Objectives use water/ oil as imaging medium for live cell imaging depending on the application.

1.4.2 Magnification

Magnification is the measure of magnifying capability of the microscopic system. Magnification can be calculated by taking the ratio of size of an image to the size of the sample. The compound microscope magnifies the image at two stages where the objective projects a magnified image into the body tube of the microscope and the eye piece further magnifies the image. The total magnification is given by:

Total Magnification = Objective Magnification   x   Eyepiece Magnification

The range of total useful magnification for the combination of objective and eyepiece is determined by the numerical aperture of the system. Basically the minimum magnification is 500xNA and the maximum useful magnification is 1000xNA. The wave nature of light imposed on the objective by diffraction sets this limit. Beyond this useful magnification will yield no additional useful information and this magnification is termed as 'Empty magnification' where increasing the magnification image magnification with no further increase in resolution.

1.4.3 Numerical aperture and Resolution

Numerical aperture (NA) of microscope objective is the measure of its ability to collect light and to resolve fine specimen detail while working at a fixed object or specimen distance [11]. It describes the acceptance cone of objective.
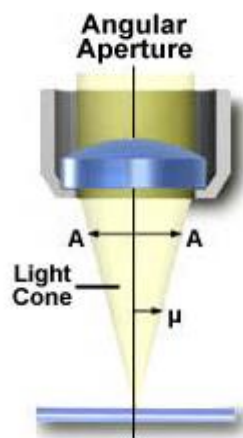

Figure 1-2: Numerical Aperture [12]

In optical microscopy the numerical aperture of optical system is given by:

$$NA = \eta \sin (\mu) \tag{1.2}$$

Where η is refractive index of medium in which lens is working and μ is half-angle of the maximum cone of light that enters or exits the lens. NA gives the resolving power of the lens.

Resolution of an optical microscope is defined as the smallest distance between two points on a specimen that can be distinguished as two separate entities. Resolution is dependent on the numerical aperture of the system. The higher the NA the better the resolution. It is given as:

$$Resolution = 0.61 * wavelength / (2 * NA)$$

1.4.4 Optical Aberrations

Aberrations are the errors in image that occur due to imperfect lenses. Aberrations lead to the blurring of the image formed by the optical system. There are different types of aberrations, spherical aberration, chromatic aberration and astigmatism.
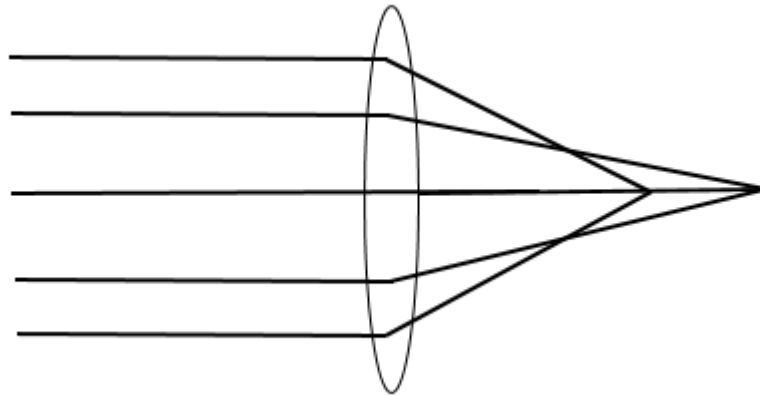
Figure 1-3: Spherical Aberration

Due to spherical aberration, paraxial rays are focused at a different distance than the point at which rays near to the principle axis are focused. This results in less quality image with degraded clarity and sharpness of the image. By using parabolic lenses spherical aberration can be avoided wherein all the rays passing through the lens meet at the focus point. Modern microscopes use special lens to avoid spherical aberration. Chromatic aberration is another optical defect that results as white light is composed of different wavelengths. These aberrations are wavelength dependent artifacts that arise due to the variation of optical glass refractive index with wavelength. Hence, different wavelengths in white light are refracted differently when passed through lens. Blue light is refracted to the greater extent followed by green and red lights. We can observe this in Figure 1.4 below.
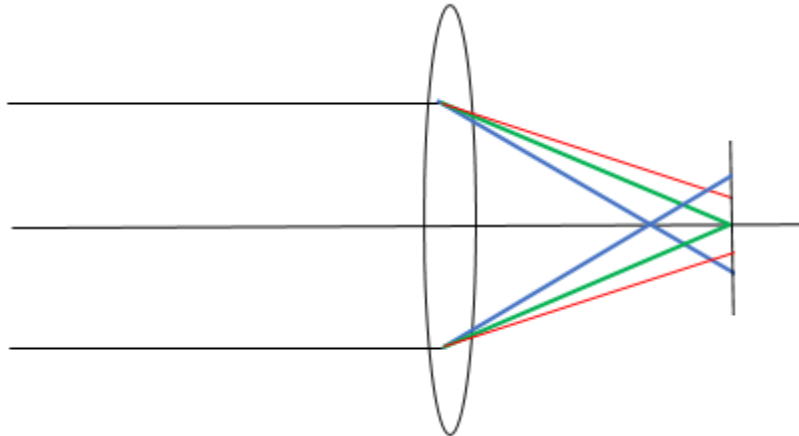
Figure 1-4: Chromatic Aberration

Astigmatism is a type of aberration that is manifested when optical system lacks cylindrical symmetry. The focus of rays is in different directions which is a result of asymmetrical lens. Comatic aberration is another kind of aberration that occur due to off-axis light fluxes. This can be partially corrected by tilting the lens. Field curvature aberration results in wave field curvature when plane field is passed through the curved lens. A flat field microscopic objective is used in modern microscopes to correct the field curvature aberration. It is always better to correct the aberrations to avoid image distortions and to get a clear image.

1.5   Optical microscopic techniques

The history of microscopy started with Dutch lens grinders Hans Janssen and his son Zacharias Janssen made the first microscope by placing two lenses in a tube, in 1590 [13]. In 1609 Galileo Galilei developed a compound microscope by using concave and convex lens. Later in 1665 documented a wide range of observations using compound microscope about the pores in a cork. In 1674 Anton Van Leeuwenhoek observed blood, insects and he was the first to describe about cells and bacteria using his microscope. Later in 1870s, Ernst Abbe formulated the relationship that resolution is correlated with the wavelength of incident light.

1.5.1   Bright field microscopy

Bright filed microscopy is the simplest and oldest microscopic technique where in, sample is observed as dark contrast against bright background which is obtained by the absorption of light by the specimen. This technique can be used to observe fixed as well as live cells. Living biological cells are phase objects and area transparent in nature. The contrast would be very low due to this transparent nature. For improving contrast between the sample and

9

background, staining is employed which may result in artifacts like damage to the live cells and finally the cells would be dead. Phase objects cannot be visualized clearly using bright field microscopy. Amplitude objects can be imaged with better contrast using this technique. Resolution achievable by using this technique is limited to 0.2μm.

1.5.2 Dark field microscopy

In dark field microscopy, we obtain a bright sample image against a dark background. The image contains only the diffracted light as a filter is used to remove the non-diffracted light. With this technique we can image bacteria, flagella, actin filaments, microtubules and unstained specimen. The image is formed due to the scattering of light by the sample. The bright field and dark filed microscopy techniques are not useful for imaging the phase objects like living biological cells.

1.5.3 Phase contrast microscopy

In 1930s Fritz Zernike came up with the invention of phase contrast microscopy where in, the phase information is represented as intensity variation. Phase objects are those that do not absorb light and they change the phase of the light diffracted by the specimen. So, when light is passed through the biological sample, the direct zeroth order light passes undeviated through and around the specimen but there will be slight change reduction in amplitude. The diffracted light wave lags behind the undiffracted wave by $\lambda/4$. Phase ring that introduces phase delay of $\lambda/4$, if introduced to the diffracted light, then there would be $\lambda/2$ phase difference between the diffracted and undiffracted waves. These waves interfere destructively and forms a dark sample against a bright background giving a much more contrast between the sample and background. This is the principle of Zernike's phase contrast microscopy. Another way to increase the contrast is to arrange the phase ring such that it slows down the direct undiffracted light there by maintaining zero phase difference between the two waves that results in bright image against a dark background. This microscopic technique is not suitable for thick specimens they appear distorted when observed under phase contrast microscopy. This disadvantage can be eliminated by using differential interference contrast microscopy (DIC).

1.5.4 Differential interference contrast microscopy (DIC)

George Nomarski, in 1950s, developed the DIC microscopy where in, a polarizer is placed after the illumination source. The task of polarizer is to convert the unpolarized light into polarized light where the light oscillates in particular direction. Then polarized light is split into two rays by using a Wollaston prism. One of the two rays passes through the specimen and the other acts as background. One ray vibrates along the axis of the prism and the other oscillates perpendicular to the first ray. MO is placed after the specimen. The two rays after

passing through MO are brought together by using another Wollaston prism. One more polarizer is used to make the two rays to vibrate in same plane and axis that results in interference of these rays. The obtained contrast depends on the thickness and refractive index of the specimen. Compared to phase contrast microscopy, DIC provides better resolution and contrast. It can be used for imaging thick specimens. Phase contrast microscopy is preferable for thin specimens whereas DIC is not preferable to calculate thickness of the object as it renders a pseudo 3D view.

All the above techniques doesn't need any extraneous contrast agents to get the phase variations or any other information about the sample. There might be intrinsic contrast agents in the specimen but there is no necessity in adding extraneous contrast agents.

1.5.5 Fluorescence microscopy

Fluorescence occurs when specimen absorbs light of particular wavelength and emits light of another higher wavelength. In fluorescence microscopy, fluorescent dyes are used as contrast agents that increases the contrast between different elements of the specimen. In bio-imaging applications, these contrast agents assists biologists to observe desired locations of different parts in a cell. For instance, Green fluorescent protein (GFP) helps to observe the location of particular proteins in a cell. Other applications of fluorescent microscope are the analysis of single molecule proteins, in vivo tracking of immune cells using fluorescent labels, to study single molecule in living cells using quantum dots [14]. The major disadvantage using fluorescent microscopy technique is the usage of fluorescent dyes cause toxicity to the biological specimen. There by, inhibiting the live cell imaging for longer periods of time. The resolution is diffraction-limited. Image is blurred due to fluorescence from out-of-focus regions of the specimen.

1.5.6 Confocal microscopy

The first confocal microscope was built by a Harvard post-doc fellow Minsky in 1957. Unlike in fluorescent microscopy where the emission comes from the complete thickness of the specimen that contains the out of focus information, in confocal microscopy the information from only the focus is obtained by using a spatial filter which eliminates out of focus information. Horizontal scanning is done to obtain the stacks of data, layer by layer, and then by using reconstruction algorithms, 3D structure of the sample can be obtained. Confocal microscopy has an advantage of better resolution compared to fluorescence microscopy, as we get secondary fluorescence from out of focus regions in fluorescence microscopy, which is not observed in confocal microscopy. Thus resulting in better resolution.

The above optical imaging techniques such as bright field, drakfield phase contrast, DIC and flourescence are useful for qualitative analysis of biological samples and there is no

feasibility of retrieving the quantitative phase information. We cannot calculate estimate the parameters like thickness of the specimen, refractive index and volume of the specimen without any quantitative information. Eventhough the confocal microscope can estimate the above parameter it takes longer time for a single image due to its scanning procedure. Quantitative phase imaging techniques render the phase information quantitatively that could be used to calculate various parameters that define the dynamics of the sample.

1.6   Quantitative Phase Imaging (QPI) techniques

Quantitative phase imaging techniques helps in obtaining the phase information quantitatively. QPI combines the ideas of Abbe's interference phenomenon [15], Zernike's image contrast [16, 17] and Gabor's Holography [18] .The measured image in QPI is a map of optical path-length shifts associated with the specimen. These images give quantitative information about the local thickness, refractive index and volume of the sample. Also the QPI techniques can give better contrast without any additional markers of staining agents. The main figures of merit in QPI are: acquisition rate, transverse resolution and phase sensitivity both temporally and spatially [19]. There are many QPI methods to retrieve phase information quantitatively like, off-axis QPI methods namely, Digital holographic microscopy (DHM) and Hilbert phase microscopy (HPM) where in, phase information is extracted from a single recorded intensity pattern using a tilted reference beam. There are phase-shifting QPI methods namely, Optical quadrature microscopy (OQM) where three or more intensity pattern are recorded to extract phase. There are common-path QPI methods namely, Fourier phase microscopy (FPM) and Diffraction phase microscopy (DPM), where in, the object and reference beam travel the same optical path. There are white-light QPI methods namely, Spatial light interference microscopy (SLIM), instantaneous Spatial light interference microscopy (iSLIM), QPI using Transport of Intensity Equation (TIE) and White-light diffraction phase microscopy (wDPM).

1.6.1   Digital Holographic Microscopy (DHM)

Digital holographic microscopy (DHM) is an off-axis QPI method where the a CCD is used to record the hologram digitally, that is formed by the interference of object beam and reference beams which follow different paths using Mach-Zehnder interferometric principle [20]. The reconstruction is done computationally to obtain the three dimensional quantitative phase information. DHM is a very useful tool in cell biology studies.

1.6.2 Hilbert Phase Microscopy (HPM)

HPM is an off-axis quantitative phase imaging technique that is similar to DHM. HPM is specifically used for imaging thin specimens like cells. Here the interferogram is recorded in the image plane instead of out-of-focus plane. There is a requirement of recording only one interferogram. As such the acquisition time is limited only by the recording device. Using HPM, live cell dynamics can be visualized to nanometer scales [21]. The acquisition time is of milliseconds range and it is useful for quantifying cell membrane fluctuations cytoskeletal dynamics and neural activity as these processes takes place in millisecond time intervals.

1.6.3 Optical Quadrature Microscopy (OQM)

Optical quadrature microscopy is a phase-shifting based quantitative phase imaging technique. OQM consists of phase-shifting Mach-Zehnder interferometer with polarizers and four cameras to record simultaneously for all four phase shifts 0, $\pi/2$, π, and $3\pi/2$ instead of independent intensity measurements. Phase information is calculated with these four recordings. This drastically reduces the acquisition time [22]. OQM is used for counting the number of cells in embryo.

1.6.4 Fourier Phase Microscopy (FPM)

Fourier phase microscopy is a common-path interferometric quantitative phase imaging technique that combines the principles of phase contrast microscopy and phase shifting interferometry. The scattered and unscattered light from the sample are used as object and reference fields of interferometer respectively. Phase is calculated from the four interferograms recorded by changing the phase of unscattered light in steps of 0, $\pi/2$, π and $3\pi/2$ with the help of programmable phase modulator [23]. Phase is obtained from these four interferograms. FPM is used to measure nanoscale fluctuations in the membrane of erythrocytes with time scales from few seconds to hours.

1.6.5 Diffraction Phase Microscopy (DPM)

Diffraction phase microscopy is a quantitative phase imaging technique that combines the idea of HPM's single shot feature with the common-path geometry associated with FPM. Due to off-axis geometry, DPM has fast acquisition rates and common-path geometry accomplishes high temporal phase sensitivity [24, 25]. The A spatial filter is used to filter out the zeroth and first order diffraction orders of the light from multiple diffraction orders generated by the grating placed at the image plane. Finally the interference pattern of the zeroth and first orders is recorded in CCD from which phase information is calculated. DPM is used for live red cell imaging, neuron cell imaging, imaging of malaria infected RBC's [26].

1.6.6 Spatial Light Interference Microscopy (SLIM)

Spatial light interference microscopy is a white-light QPI method in which offers high temporal stability due to common-path geometry, high spatial stability due to white-light illumination and high transverse resolution that is provided by the phase-shifting principle. Here four interferograms are recorded by shifting the phase of unscattered light from the sample with respect to scattered light in the order of 0, $\pi/2$, π, and $3\pi/2$. Then the phase is reconstructed using these four interferograms [27]. Though the acquisition rates are low as we need to record four interferograms, it removes the speckle noise which is observed in DPM where high coherent laser has been used as source of illumination.

1.6.7 Instantaneous Spatial Light Interference Microscopy (iSLIM)

Instantaneous spatial light interference microscopy is a quantitative phase imaging technique that combines the benefits of white light phase contrast microscopy and phase stability resulting from diffraction phase microscopy [28]. It has significant advantages due to whit-light illumination and common-path geometry of DPM. It has applications in measurement of cell fluctuations and mechanical properties of the cell.

1.6.8 QPI using Transport of Intensity Equation (TIE)

This is another type of white-light QPI technique that doesn't involve interferometric geometry and image filed itself acts as interferogram. Here phase is calculated by the transport of intensity equation. The amplitude and phase distributions are mathematically coupled in defocused images. By measuring intensity images around the focus, quantitative phase image of the in-focus filed is obtained [29]. Usage of white light provides spatial stability and common path geometry helps in temporal phase stability.

1.6.9 White Light Diffraction Phase Microscopy (wDPM)

White light diffraction phase microscopy is a quantitative phase imaging technique that combines off-axis and common path geometry which is similar to DPM except that it utilizes white-light illumination. It has an advantage of using white light illumination as it removes the speckle noise that is observed with laser illumination in DPM and due to off –axis geometry it needs single interferogram for reconstructing the phase. There by it has high acquisition rates compared to SLIM as it needs four interferograms for retrieving phase. The set up for wDPM doesn't require specialized phase contrast microscope optics compared with SLIM and iSLIM.

Thus *white light diffraction phase microscopy (wDPM)* is an emerging quantitative phase imaging technique that gives the nanoscale spatial as well as temporal stability with less noise. In this work We have deisgned and developed the wDPM set up and recorde the interferogram. We implemented a fast phase reconstruction algorithm to retrieve the phase

of the object from the recorded interferograms. This algorithm avoids the unwrapping step which is needed in conventional phase reconstruction by Hilbert's transform method. We have demonstrated the quantitative phase imaging of sperm cells and yeast cell and calculated the thickness and also we showed the dynamics of yeast cells.

Chapter 2

Diffraction Phase Microscopy

2.1   Introduction

Fritz Zernike earned a Nobel Prize in Physics in 1957 for his invention of phase contrast microscopy in 1930s. From that time onwards, phase of light has been a vital probe for obtaining specimen morphology and topographical information [30]. Phase shifts associated with the light scattered by the specimen are related to the local optical properties-refractive index and thickness of the specimen under observation. Gabor invented a new microscopic principle – holography in 1948 for which he received the Nobel Prize in Physics in 1971. Using holography phase information can be recorded. Goodman and Lawrence were the first to demonstrate the numerical reconstruction of holograms [31]. Analysis of fringes in off-axis holography using a fast Fourier transform method has been demonstrated by Takeda et.al in 1982 [32]. Interferometry and holography play a vital role in optical metrology by providing topographical information about the sample with nanoscale accuracy [33]. In quantitative phase imaging, the optical path-length map across a specimen is measured. The main basis of QPI is that the phase of a field is much sensitive to the specimen structure than the amplitude of the field. When the source field interacts with the specimen, scattered field undergoes phase-shifts with respect to the unscattered light fields. These phase-shifts contain the information about the thickness and refractive index of the sample under investigation. Due to its promising nature of quantitative phase information, QPI has many applications in biomedicine [19]. The phase noise due to mechanical vibrations and air fluctuations affect the interferometric system. This noise is the main obstruction for retrieving phase images with high sensitivity. Diffraction phase microscopy (DPM) overcomes this noise problem as it has common-path, off-axis geometry with Mach-Zehnder interferometric system. The common-path configuration cancels out the noise inherently and single shot is required for recording the phase. So the acquisition speed is limited only by the recording device. And this technique doesn't require any staining or tagging the specimen. So, with all these features, DPM is used to monitor accurately the dynamics of biological live cells. DPM is used in various

16

applications like measuring the dynamics of biological samples, semiconductor wet etching and photochemical etching processes, surface wetting and evaporation of water droplets, expansion and deformation of materials, self-assembly of nanotubes. DPM with white light removes the speckle noise there by increasing spatial phase sensitivity.

2.2　Principles of Diffraction Phase Microscopy

2.2.1　Theory

Diffraction phase microscopy is an add-on module to the commercially available Axio Observer Z1 Zeiss. Figure 2.1 shows the schematic of the DPM system. A diffraction grating is placed at the output image plane of the microscope. It is used along with a 4f system so as to allow the interference phenomenon and obtain the phase information. From grating we obtain copies of the image at different angles. We need only 0th and 1st order beams to form the interference pattern on the CCD. This is achieved by using a spatial filter in the Fourier plane that allows only these two orders to reach the CCD plane. The 0th order
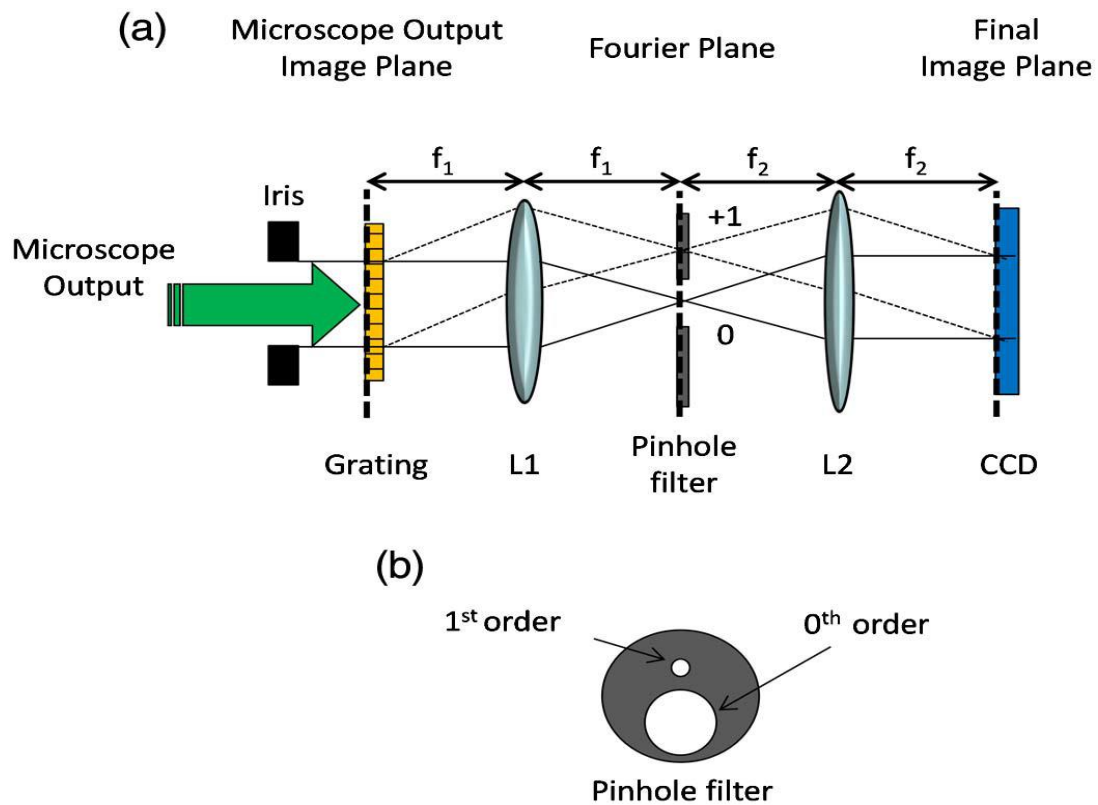

Figure 2-1: DPM schematic set up

is allowed to pass fully and 1st order is filtered using pin hole such that after L2, the field becomes uniform plane and acts as a reference in the interferogram. The two fields form the

17

final image by interference on the CCD plane to get recorded as an interferogram. We have field in the grating plane (GP) as

$$U_{GP}(x, y) = U_0(x, y) + U_1(x, y)e^{i\beta x} \qquad (2.2.1\text{-}1)$$

where U_0 is 0th order field and U_1 is $+1^{st}$ order field. $\beta = 2\pi/\Lambda$ where Λ is the grating period. The field after Fourier transforming by lens L1 i.e. before the filter in Fourier plane (FP-) is

$$\tilde{U}_{FP\text{-}}(k_x, k_y) = \tilde{U}_0(k_x, k_y) + \tilde{U}_1(k_x - \beta, k_y) \qquad (2.2.1\text{-}2a)$$

$$k_x = 2\pi x_1 / (\lambda f_1) \equiv \alpha x_1, \qquad k_y = 2\pi y_1 / (\lambda f_1) \equiv \alpha y_1, \qquad (2.2.1\text{-}2b)$$

$$\beta = 2\pi / \Lambda = 2\pi \Delta x / (\lambda f_1) \equiv \alpha \Delta x, \qquad \Delta x = \lambda f_1 / \Lambda, \qquad (2.2.1\text{-}2c)$$

where (x_1, y_1) are the coordinates in Fourier plane. Equation (2.2.1-2b) explains the relation between the angular spatial frequency variables and their actual location in free space. Here, Δx denotes the physical spacing between the 0th and 1st order diffraction patterns in the Fourier plane. The spatial filter allows only the DC component of 1st order such that after Fourier transforming again, it appears uniformly at the CCD plane and allows 0th order fully forming the image field against uniform background in the CCD plane. So, immediately after the pin hole (FP+) we have field as

$$\tilde{U}_{FP+}(\alpha x_1, \alpha y_1) = \tilde{U}_0(\alpha x_1, \alpha y_1) + \tilde{U}_1(\alpha x_1 - \beta, \alpha y_1) * \delta(\alpha x_1 - \beta, \alpha y_1)$$

$$= \tilde{U}_0(\alpha x_1, \alpha y_1) + \tilde{U}_1(0,0) * \delta(\alpha x_1 - \beta, \alpha y_1) \qquad (2.2.1\text{-}3)$$

Here $\tilde{U}_1(0,0) * \delta(\alpha x_1 - \beta, \alpha y_1)$ is the spatial frequency domain representation of DC signal and $\tilde{U}_0(\alpha x_1, \alpha y_1)$ is the unfiltered signal that provides image information. Then the lens L2 takes another forward Fourier transform that results in

$$F.T\{\tilde{U}_{FP+}(\alpha x_1, \alpha y_1)\} = F.T\{\tilde{U}_0(\alpha x_1, \alpha y_1) + \tilde{U}_1(0,0) * \delta(\alpha x_1 - \beta, \alpha y_1)\}$$

$$= \frac{1}{|\alpha|}(U_0(\xi / \alpha, \eta / \alpha) + U_1(0,0)e^{-i\xi\beta/\alpha}) \qquad (2.2.1\text{-}4a)$$

$$\xi \equiv 2\pi x / \lambda f_2, \qquad \eta \equiv 2\pi y / \lambda f_2 \qquad (2.2.1\text{-}4b)$$

Therefore the resulting field at the camera plane (CP) is given as

$$U_{CP}(x, y) = \frac{1}{|\alpha|}[U_0(-x/M_{4f}, -y/M_{4f}) + U_1(0,0)e^{i\beta x/M_{4f}}] \qquad (2.2.1\text{-}5a)$$

where $M_{4f} \equiv -f_2/f_1$ $\qquad (2.2.1\text{-}5b)$

We can write U_0 and U_1 in phasor form as

$$U_0(x, y) \equiv A_0(x, y)e^{i\phi_0(x,y)} , \quad U_1(x, y) \equiv A_1(x, y)e^{i\phi_1(x,y)} \qquad (2.2.1\text{-}6)$$

So Equation (2.2.1-5a) becomes

$$U_{CP}(x, y) = \frac{1}{|\alpha|}[A_0(-x/M_{4f}, -y/M_{4f})e^{i\phi_0(-x/M_{4f}, -y/M_{4f})} + A_1(0,0)e^{i\beta x/M_{4f}}e^{i\phi_1(0,0)}$$

$$(2.2.1\text{-}7)$$

By assuming $-x/M_{4f} \to x', -y/M_{4f} \to y', A_0/|\alpha| \to A_0', A_1/|\alpha| \to A_1'$, we can write Equation (2.2.1-7) as

$$U_{CP}(x, y) = A_0'(x', y')e^{i\phi_0(x',y')} + A_1'e^{-i\beta x'}e^{i\phi_1} \qquad (2.2.1\text{-}8)$$

We obtain the interference of two magnified images at the camera plane where both are inverted in *x* and *y*. This inversion is due to the 4f system where Fourier transform is applied twice to the light field instead of transform pair. The resultant intensity at the CCD plane is given by

$$I_{CP}(x', y') = U_{CP}(x, y)U^*_{CP}(x, y)$$

$$= |A_0'(x', y')|^2 + |A_1'|^2 + 2|A_0'(x', y')||A_1'|\cos(\beta x' + \Delta\phi) \qquad (2.2.1\text{-}9)$$

$$\Rightarrow I_{CP}(x', y') = I_0(x', y') + I_1 + 2\sqrt{I_0(x', y')I_1}\cos(\beta x' + \Delta\phi), \qquad (2.2.1\text{-}10a)$$

$$\text{So, } \Delta\phi = \phi_0(x', y') - \phi_1. \qquad (2.2.1\text{-}10b)$$

Equation (2.2.1-10b) gives the phase information from the sample that is obtained from the cosine term. This cosine term is a resultant of interference of the two diffraction orders i.e. image and reference beams.

2.2.2 Design Principles

2.2.2.1 Transverse Resolution

In DPM system, the transverse resolution of the final image is dependent on two parameters. They are optical resolution of the microscope and period of grating. The resolution is given by Abbe's formula [35] as:

$$\Delta\rho = \frac{1.22\lambda}{(NA_{obj} + NA_{con})}$$

$$\simeq \frac{1.22\lambda}{NA_{obj}}$$

<div align="right">(2.2.2-1)</div>

where NA_{obj} and NA_{con} are objective and condenser numerical apertures. It is approximated

by assuming plane wave illumination i.e. $NA_{con} \simeq 0$. The resolution using Abbe's formula

is calculated according to Rayleigh criterion. $\Delta\rho$ represents the diffraction spot radius or

the distance from the peak to the first zero of the Airy pattern. So, the resolution for DPM

system varies according to the objective employed. Higher the NA used for particular

wavelength, better the resolution of the image.

2.2.2.2 Sampling : Grating period and Pixel size

Sampling of the image is done by grating. The grating period should be sufficient such that

the sampling doesn't degrade the optical resolution of the microscope. According to the

Nyquist theorem, two periods per diffraction spot gives minimum grating period. But due to

the interference phenomenon, this number is not sufficient. Figure 2 shows the Fourier

transform of the DPM interferogram. Due to the interference central lobe radius is
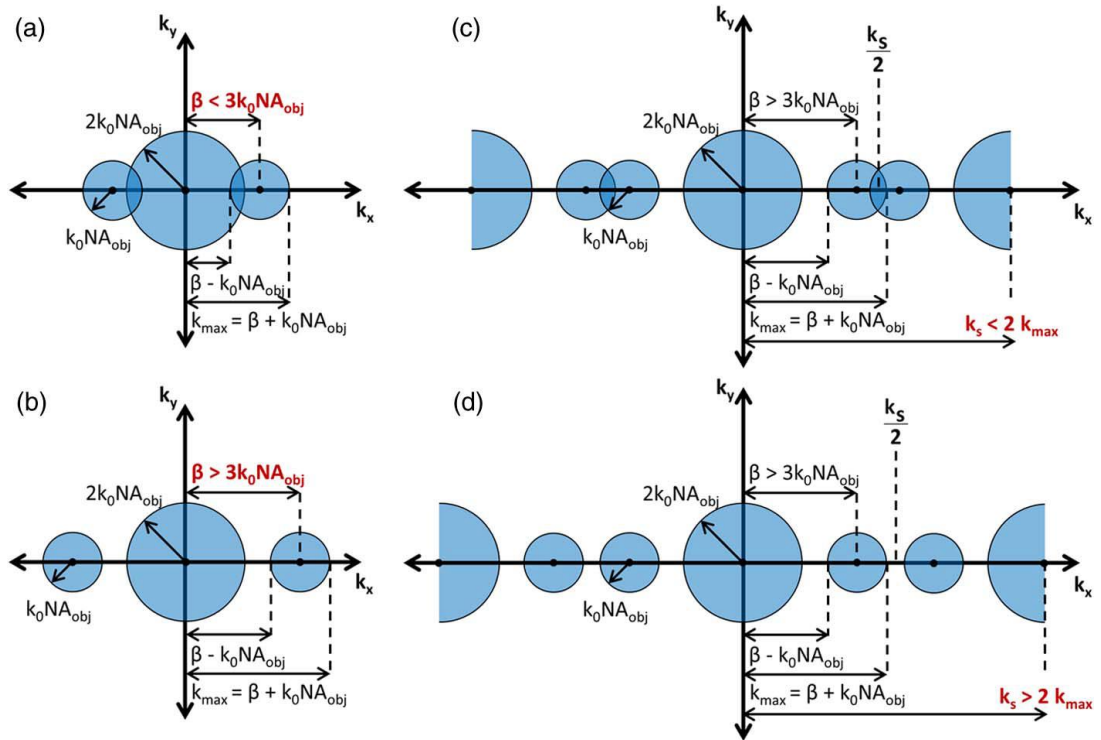

Figure 2-2: F.T of intensity at CCD plane at different conditions [34]

$2k_0NA_{obj}$ and for side lobes it is k_0NA_{obj}. To avoid aliasing effect i.e. overlapping frequencies

in Fourier plane the modulation frequency β must satisfy the following condition:

$$\beta \geq 3k_0 NA_{obj}. \tag{2.2.2-2}$$

where $\beta = (2\pi / \Lambda)M_{obj}$, Λ is grating period and M_{obj} is the magnification of the microscope. By substituting β in Equation (2.2.2-2), we obtain

$$\Lambda \leq \frac{\lambda M_{obj}}{3NA_{obj}} \tag{2.2.2-3}$$

Equation (2.2.2-3) is the basis criterion for selection of grating period. By using Equation (2.2.2-1), expressing NA_{obj} in terms of $\Delta\rho$ (diffraction spot radius), we get

$$\Lambda \leq \frac{\Delta\rho M_{obj}}{3.66} \tag{2.2.2-4}$$

So this implies that at least 3.66 grating fringes per diffraction spot radius are needed to avoid aliasing and obtain optimal resolution.

For proper sampling of interferogram, the following condition must be met.

$$k_s \geq 2k_{max} = 2(\beta + k_0 NA_{obj}) \tag{2.2.2-5}$$

where k_s is the pixel sampling frequency. If we consider the physical pixel size of the camera as a then the condition necessary to avoid aliasing due to pixel sampling is:

$$k_s = \frac{2\pi}{a} M_{obj} |M_{4f}| \geq 2(\beta + k_0 NA_{obj}) \tag{2.2.2-6a}$$

$$\Rightarrow |M_{4f}| \geq 2a \left[\frac{1}{\Lambda} + \frac{1}{\lambda} \frac{NA_{obj}}{M_{obj}} \right] \tag{2.2.2-6b}$$

$$\Rightarrow |M_{4f}| \geq \frac{8a}{3\Lambda} \tag{2.2.2-6c}$$

So, Nyquist condition will be satisfied only if Equations (2.2.2.3) and (2.2.2-6c) holds good. Figure 2(a) shows the aliasing effect as a result of large grating period. Figure 2(b) shows Fourier transform where grating period is small enough to avoid aliasing. Figure 2(c) explains that sampling doesn't meet Nyquist criterion even though the grating period is chosen correctly. This again results in aliasing effect. Figure 2(d) shows no aliasing effect as the two requirements for Nyquist criterion are met.

2.2.2.3 Field of View

The field of view in the sample plane for an *m X n* image is calculated as:

$$FOV = [m,n] \frac{a}{M_{obj} |M_{4f}|} \tag{2.2.2-7}$$

where a is the physical pixel size of the camera, M_{obj} is magnification of the objective and M_{4f} is magnification of 4f system.

2.2.2.4 Fourier plane spacing (Filter construction)

The grating period affects the physical spacing in Fourier plane. The basic grating equation for mth diffraction order at normal incidence is

$$\sin(\theta_m) = m\frac{\lambda}{\Lambda} \tag{2.2.2-8}$$

Distance from grating to the lens L1 is f_1 and the separation between 0th and 1st order beams is Δx that is nearly constant after passing through L1.

$$\text{So, } \tan(\theta_m) = \frac{\Delta x}{f_1} \tag{2.2.2-9}$$

We know that for very small angles, we can approximate as

$$\tan(\theta_m) \approx \sin(\theta_m) \approx \theta_m$$

So, Equation (2.2.2-8) gives the following:

$$\Delta x = \frac{f_1\lambda}{\Lambda} \tag{2.2.2-10}$$

This is used to design the physical pinhole in the spatial filter. Δx should be smaller than f_1 so that 0th and 1st orders fit through the lens L1and 0th order to pass through the center of the lens. This condition is satisfied when the below criteria holds good.

$$NA_{L_1} \geq \frac{\lambda}{\Lambda} + \frac{NA_{obj}}{M_{obj}} \tag{2.2.2-11}$$

2.2.2.5 Pinhole size (Uniform reference at CCD plane)

The pinhole acts as a low-pass filter that allows only the DC component of 1st order. The size of the pinhole should be chosen such that the reference beam is uniform all over the FOV of CCD. A larger cut can be used for 0th order. A plane wave passing through the pinhole filter of diameter D after L2 performs a Fourier transform has the Fraunhofer diffraction pattern in the form

$$I(x, y) = I_0 \left[\frac{2J_1(\pi D\rho / \lambda f_2)}{\pi D\rho / \lambda f_2} \right]^2 \tag{2.2.2-12}$$

where J_1 is a Bessel function of first kind, I_0 is the peak intensity, f_2 is the focal length of lens L2, $\rho = \sqrt{x^2 + y^2}$ and λ is the mean wavelength of the illumination [36].

We can solve for the radius ρ of the central lobe by equating the argument of the jinc function to the location of the first zero.

$$\text{i.e. } \frac{\pi D \rho}{\lambda f_2} = 3.83 \tag{2.2.2-13a}$$

$$\Rightarrow \rho = 3.83 \frac{\lambda f_2}{\pi D} = 1.22 \frac{\lambda f_2}{D} \tag{2.2.2-13b}$$

The diameter of the central lobe of the jinc function should be much larger, by a factor of γ than the diagonal dimension of the CCD sensor. This allows the reference beam to be uniform across the image. CCD has square pixels and rectangular sensor, so the diagonal distance d used in this calculation:

$$d = a\sqrt{m^2 + n^2} \tag{2.2.2-14a}$$

$$\rho = 1.22 \frac{\lambda f_2}{D} \geq \frac{\gamma d}{2} \tag{2.2.2-14b}$$

$$D \leq \frac{2.44 \lambda f_2}{\gamma d} \tag{2.2.2-14c}$$

The above condition is used to design the pinhole diameter. It designed depending on the mean wavelength of illumination, focal length of lens L2, diagonal distance of the CCD sensor and we take $\gamma = 4$. Smaller pinhole yields a uniform reference but intensity is reduced. The pinhole should be small enough to render uniform reference across the image while maintaining reasonable intensity to visualize the fringes. Using a blazed grating will serve this purpose. For the 0th order and filtered 1st order to pass through the lens L2 completely, the following condition should be satisfied.

$$NA_{L_2} \geq \frac{\lambda}{\left| M_{4f} \right| \Lambda} + \frac{1.22\lambda}{D} \tag{2.2.2-15}$$

Completely passing the both diffraction orders is not absolute necessary condition. But the two orders just need to overlap in the CCD plane to cover the field of view and the feasible condition for this to happen is:

$$NA_{L_2} \geq \frac{\lambda}{\left| M_{4f} \right| \Lambda} + \frac{1.22\lambda}{\gamma D} \tag{2.2.2-16}$$

The degree of coupling between unscattered and scattered beams is determined by the figure of merit which is the ratio of unscattered and scattered light beam radii in Fourier plane. It is expressed as:

$$\eta = \frac{1.22 \lambda M_{obj} \left| M_{4f} \right|}{a \sqrt{m^2 + n^2} \, NA_{obj}}$$

(2.2.2-17)

This ratio should be ideally minimal in order to properly reconstruct the quantitative phase image. The above ratio can be expressed in the sample plane as the ratio of diffraction spot radius to the FOV diagonal diameter as follows:

$$\eta = \frac{\Delta \rho}{FOV_{diagonal}}$$

(2.2.2-18)

$\eta = 1$ implies that diffraction spot is equal to FOV and we obtain only DC signal. As $\eta \to 0$ we can observe more details of the image within the given FOV.

All the design equations required for DPM system are summarized in the below table. So, for better designing of DPM system, a correct combination of diffraction grating, 4f lenses and pinhole filter are to be chosen. There should be at least 2.67 pixels per fringe and 3.6 fringes per diffraction spot radius. The grating period is selected based on the objective and the magnification of 4f lenses is determined by the grating period and pixel size of camera. This determines the FOV. The numerical aperture of the lens L1 should be selected such that the two orders fit through the lens L1. The NA for L2 should be large to capture the both 0th and 1st order beams. The pin hole should be chosen in such a way that the resultant diffraction pattern has large central lobe at CCD plane for yielding uniform reference image.

Table 1: DPM design equation [34]

Equation	Description
$\Delta\rho = \dfrac{1.22\lambda}{NA_{obj}}$	Resolution (diffraction spot radius)
$\Lambda \leq \dfrac{\lambda M_{obj}}{3NA_{obj}}$	Maximum grating period (separated orders)
$\left\| M_{4f} \right\| \geq 2a\left[\dfrac{1}{\Lambda} + \dfrac{1}{\lambda}\dfrac{NA_{obj}}{M_{obj}} \right]$	Minimum 4f magnification (sampling)
$M_{4f} = \dfrac{-f_2}{f_1}, M = M_{obj}M_{4f}$	Magnification
$FOV = [m,n]\dfrac{a}{M_{obj}\left\| M_{4f} \right\|}$	Resulting FOV in sample plane
$\Delta x = \dfrac{f_1\lambda}{\Lambda}$	Fourier plane spacing (filter design)
$NA_{L_1} \geq \dfrac{\lambda}{\Lambda} + \dfrac{NA_{obj}}{M_{obj}}$	Minimum NA for lens L1 (avoid clipping)
$D \leq \dfrac{2.44\lambda f_2}{\gamma d}$	Maximum pinhole diameter (uniform reference beam)
$NA_{L_2} \geq \dfrac{\lambda}{\left\| M_{4f} \right\|\Lambda} + \dfrac{1.22\lambda}{D}$	Minimum NA for lens L2 (avoid clipping)
$\eta = \dfrac{1.22\lambda M_{obj}\left\| M_{4f} \right\|}{a\sqrt{m^2 + n^2}\, NA_{obj}} = \dfrac{\Delta\rho}{FOV_{diagonal}}$	Coupling ratio (ratio of DC to AC)

Chapter 3

White Light Diffraction Phase Microscopy

Due to usage of laser light as source of illumination in DPM, the images obtained suffer from speckles which in turn degrades spatial phase sensitivity. Whit light diffraction phase microscopy (wDPM) is an emerging quantitative phase imaging technique that white light as source of illumination there by improves the spatiotemporal noise of the system [37]. This low noise is due to the use of low coherence light both spatially and temporally. Laser DPM is preferred for material science applications where as white light DPM is the best technique that has many biological applications [38, 39]. Each type of illumination has its own advantages and drawbacks.

3.1   Design

MO used in wDPM has 0.75 NA and magnification factor of 40x. The diffraction spot radius is calculated by using Equation (2.2.2-1).For   of 532nm, we obtain the diffraction radius spot to be approximately 865 nm. Grating period should be such that it avoids aliasing by separating 0th and 1st orders and provide better optimal resolution. So, by using the diffraction spot radius the maximum grating period is calculated using Eq.(2.2.2-4).The maximum grating period is 9.5μm. We have set the grating period to be 9 μm. Necessary condition to avoid aliasing due to pixel sampling is   . We have used UI-1482LE-M camera that has pixel size a of 2.2 μm, optical sensor diagonal d of 7.04mm and resolution 2560 x 1920. So, the minimum 4f magnification required is 0.65. In our wDPM set up, we have used lenses L1, L2 of focal lengths 50mm, 125mm for relaying the image plane IP1 to plane IP2 and L3 and L4 of focal lengths 60mm and 100mm for 4f system. So the magnification given by L1 and L2 lenses is 2.5and by L3 and L4 lenses is 1.67. The final magnification M is 4.17. The resulting FOV is given by Eq.(2.2.2-7) where [m, n] is [2560, 1920] . So the FOV is [1.35mm, 1.02mm]. The separation between 0th and 1st order beams is   which is given by

Eq.(2.2.2-10). So, in filter design the Fourier spacing is calculated to be 3.5mm.To avoid clipping, minimum NA required for lens L3 is given by Eq.(2.2.2-11) and is found to be 0.08. The maximum pin hole diameter for uniform reference beam is given by Eq.(2.2.2-14c). We have the value for diagonal distance of our camera to be 7.04mm. So, the maximum pin hole diameter is 4.6μm. The minimum NA required for lens L4 is given by Eq.(2.2.2-15) and is found to be 0.17.

3.2   Methodology

Figure 3.1 shows the experimental set up for white light diffraction phase microscopy. It is an add-on module to the commercially available microscope, Axio Observer Z1, Zeiss. A halogen lamp acts as source of white light illumination. The condenser aperture is set to minimum possible value i.e., NA=0.09 so as to make the entire light in the field of view spatially coherent. During the whole process of experiment we operate the microscope in bright filed mode with 40x (0.75 NA) objective. The image is formed at the image plane IP1 outside the inverted microscope. We have used a 4f system (lenses L1, L2) to replicate the microscopic image at plane IP2. We employed reflective spatial light modulator (SLM) that serves the purpose of diffraction phase grating G, in the image plane IP2 with 9μm grating period such that it is smaller than the diffraction-limited spot of the microscopic imaging system at the grating plane. This diffraction grating renders multiple diffraction orders that has full spatial information about the specimen. The two diffraction orders, zeroth and first, are filtered out at the Fourier plane of lens L3. The zeroth order is spatially low-pass filtered through the pin hole such that only DC component of zeroth order is allowed and the diameter of the pin hole is typically maintained at 200μm. The entire frequency content of first diffraction order is allowed to pass through the first order mask which is a rectangular opening, typically of the size 5x2 mm^2, in the aluminum foil. The lenses L3-L4 forms a highly stable Mach-Zehnder interferometer. The first order plays the role of imaging field and zeroth order plays the role of reference field. Then after the two diffraction orders are inverse Fourier transformed by passing through the lens L4, they interfere and generate a spatially modulated interference image. This interferogram is recorded using a CCD camera.

3.3   Phase Reconstruction

Hilbert's transform based method and Fast Phase reconstruction methods are used for phase reconstruction. The spatially varying irradiance for a given sample at the image plane across either x or y axis has the form

$$I(x) = I_R + I_s(x) + 2[I_R I_s(x)]^{1/2} \cos[qx + \phi(x)] \qquad (3.3\text{-}1)$$

where I_R and I_s are reference and sample irradiance distributions respectively, q is spatial frequency of the fringes and ϕ is the spatially varying phase associated with the object [40]. The sinusoidal term $u(x) = 2[I_R I_s(x)]^{1/2} \cos[qx + \phi(x)]$ can be isolated by Fourier high-pass filtering. It follows that the complex analytical signal associated with the real function $u(x)$ can be obtained as:

$$z(x) = \frac{1}{2}u(x) + i\frac{P}{2\pi}\int_{-\infty}^{\infty}\frac{u(x')}{x-x'}dx' \qquad (3.3\text{-}2)$$
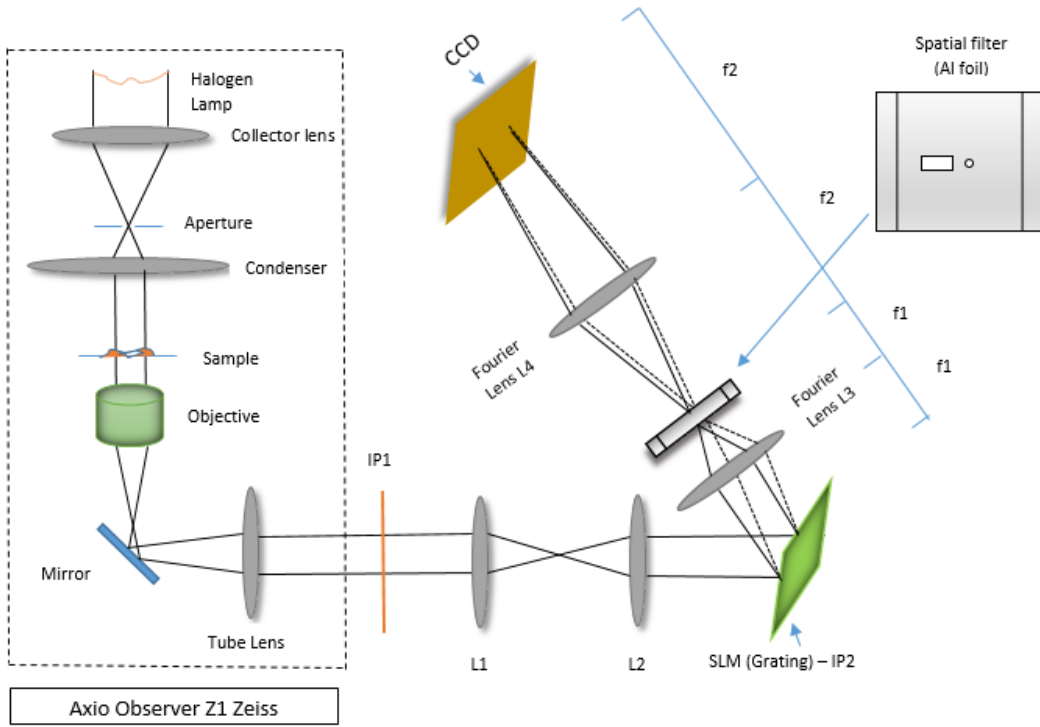
Figure 3-1: wDPM schematic set up

In Eq.(3.3-2), the imaginary part of the right-hand side stands for a principal-value integral, which is easily identified as Hilbert transform of $u(x)$. Hence, the phase associated with complex analytical signal z is calculated as $\Phi(x) = \tan^{-1}\{\mathrm{Im}[z(x)]/\mathrm{Re}[z(x)]\}$. z exhibits rapid phase modulation with frequency q, hence Φ is strongly wrapped. As q is higher than the spatial frequency content of the object, the unwrapping algorithm is used. Finally, the phase associated with the object is extracted as $\phi(x) = \Phi(x) - qx$. The algorithm for reconstruction using Hilbert's transform based method is shown in below flowchart.
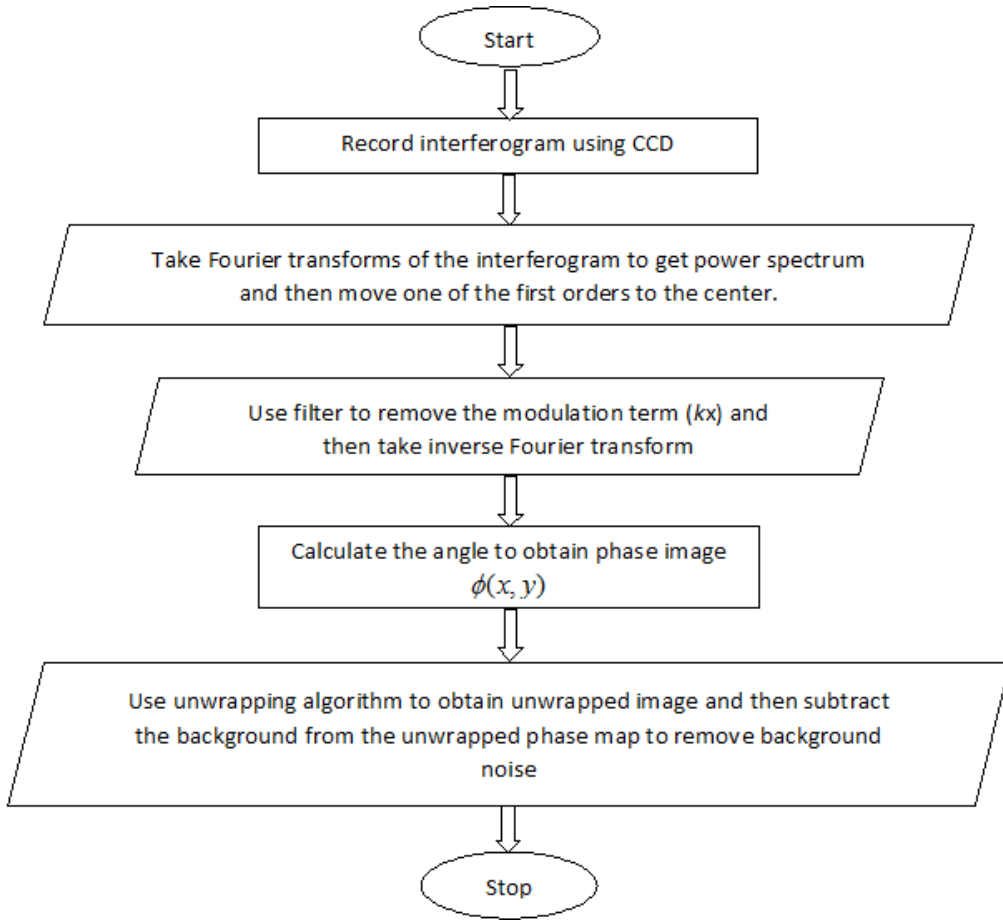
In our experiment, the quantitative phase image of the sample is retrieved from the recorded interferogram using a fast phase reconstruction algorithm that bypasses the need for unwrapping step that is necessary in conventional Hilbert's transform based reconstruction method [41]. As the unwrapping step is not needed, the phase reconstruction can be done rapidly. At the beginning of the experiment we capture the background interferogram only once, as the phase of the background doesn't change for particular specimen-holder. This background information is used for all the subsequent images. The intensity distribution of the interferogram at the CCD by taking into consideration the background and noise is:

$$I(x, y) = \left|U_i(x, y)\right|^2 + \left|U_r\right|^2 + 2.\left|U_r\right|\left|U_i(x, y)\right|\cos[kx + \phi(x, y) + \varphi_{bg}(x, y) + \varphi_n(x, y)]$$

(3.3-3)

where $\left|U_i(x, y)\right|$ is the imaging field, $\left|U_r\right|$ is the reference field, k is the grating period, $\phi(x, y)$ is the phase delay introduced by the sample, $\varphi_{bg}(x, y)$ is the phase shift introduced by the background and $\varphi_n(x, y)$ is the noise.

We Fourier transform the Equation (3.3-3), shift first order to the center and perform the inverse Fourier transform, then the resultant term is:

29

$$2|U_r||U_i(x, y)|.\exp[i(\Delta\phi(x, y)+\varphi_{bg}(x, y)+\varphi_n(x, y))] \qquad (3.3\text{-}4)$$

When there is no phase object in the field of view, Equation (3.3-3) becomes:

$$I(x, y) = |U_i(x, y)|^2 + |U_r|^2 + 2.|U_r||U_i(x, y)|\cos[kx+\varphi_{bg}(x, y)+\varphi_n(x, y)] \qquad (3.3\text{-}5)$$

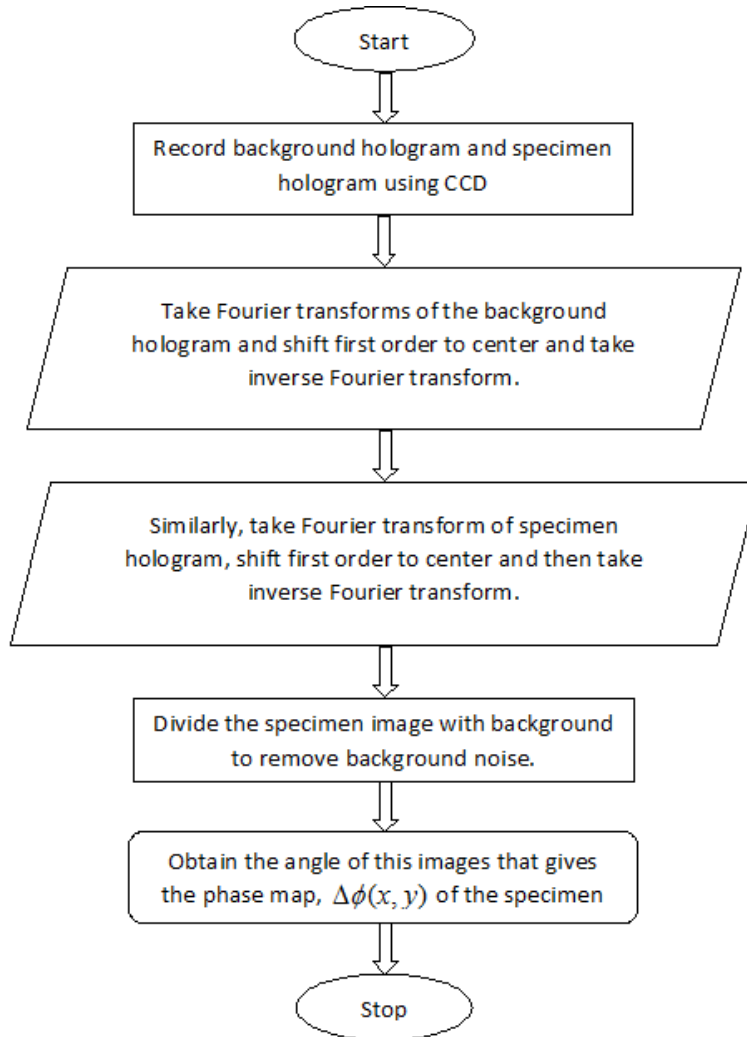By following the same process done to Equation (3.3-3), the resultant term for Equation (3.3-5) is:

$$2|U_r||U_i(x, y)|.\exp[i(\varphi_{bg}(x, y)+\varphi_n(x, y))] \qquad (3.3\text{-}6)$$

Dividing Equation (3.3-4) by Equation (3.3-6), we get the term

$$\exp[i\Delta\phi(x, y)] \qquad (3.3\text{-}7)$$

Hence, by taking the angle of Equation (3.3-7), we retrieve the phase map $\Delta\phi(x, y)$ associated with the sample.

The following flow chart explains the fast phase reconstruction algorithm.


30

Chapter 4

Experimental Results

We have recorded the phase map of yeast cells and sperm cells. Yeast cells were grown in YPD broth (Yeast extract 1%, peptone 2% and dextrose 2%) till log phase. We have extracted yeast cells for imaging using wDPM technique while they are in log phase. We have used the fast phase reconstruction algorithm for retrieving phase information. We employed UI-1482LE-M camera that has pixel size a of 2.2 µm, optical sensor diagonal d of 7.04mm and resolution 2560 x 1920. We have recorded the hologram of yeast cells and take the Fourier transform which shows the 0th and 1st order frequencies. Then we select the 1st order frequency and shift it to center then inverse Fourier transform is applied. All these steps are shown in Fig.4-1. We have recorded only once the interferogram of the background image, as the phase of the background doesn't change for particular specimen-holder. This information is used for all subsequent images. The resultant interference pattern due to the 0th and 1st order beams is shown in the zoomed part of the background hologram. The similar steps for background hologram are shown in Fig.4-2. The amplitude and phase of hologram for yeast cells is shown in Fig.4-3 (a) and (b). The amplitude and phase of the background image are shown in Fig. 4-3 (c) and (d). The curvature aberrations observed in phase map are due to the usage of MO in the optical path. These aberrations can be removed by dividing the specimen with the background as these aberrations also appear in the phase map of specimen. The phase map, $\Delta\phi(x, y)$, for yeast cells is obtained by calculating the angle after dividing the inverse Fourier transformed yeast cells with inverse Fourier transformed background image. This implies background subtraction which removes much of the background noise and aberrations which occur due to MO. Figure 4-4 shows the phase map of yeast cells.
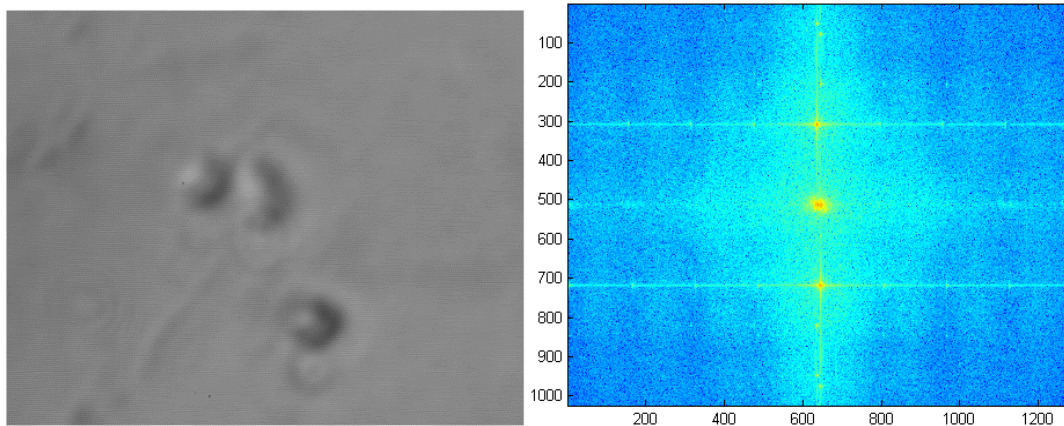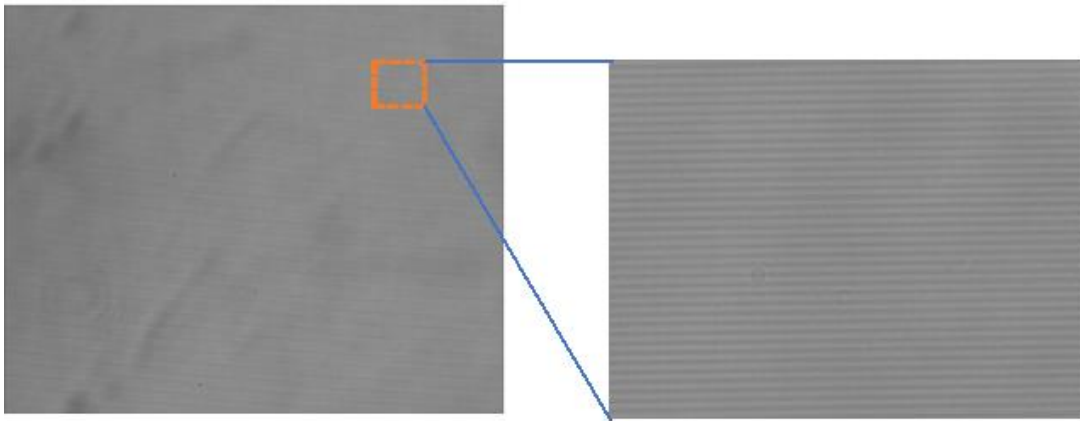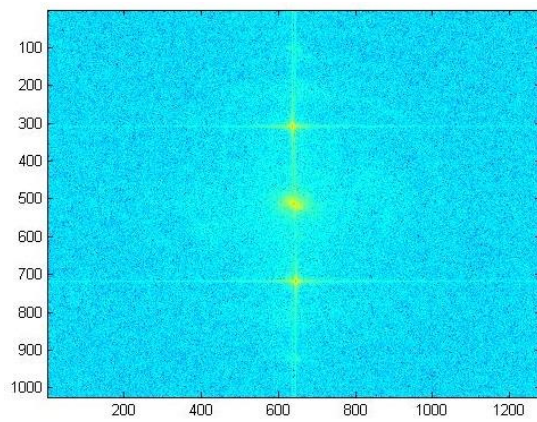
(a)

(b)
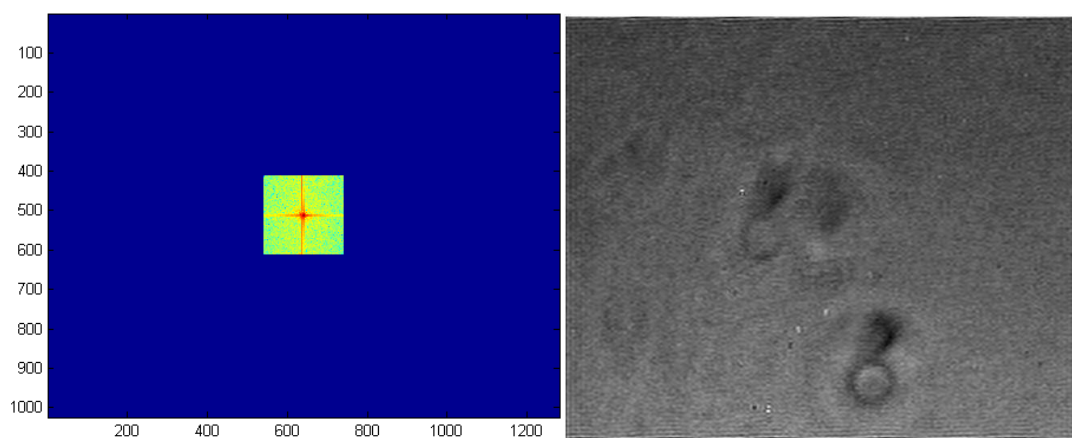
(c)

(d)

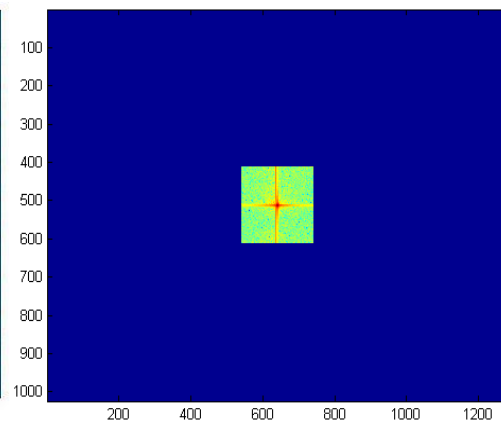**Figure 4-1: (a) Hologram of yeast cell   (b) Fourier Transform for(a)**

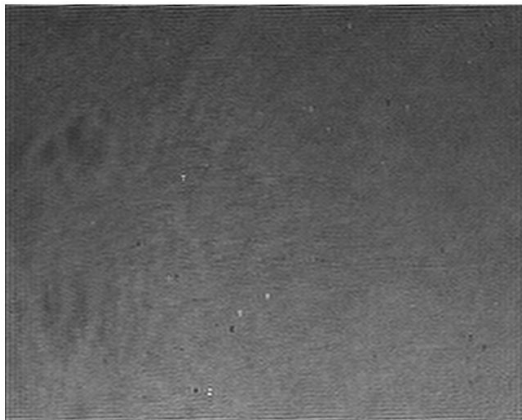**(c) First order shifted to center (d) Inverse Fourier Transform of (c)**

(a)

(b)

(c)

(d)

Figure 4-2: (a) Background interferogram without any specimen (b) Fourier Transform of Background interferogram (c) First order shifted to center (d) Inverse Fourier transform of background hologram.
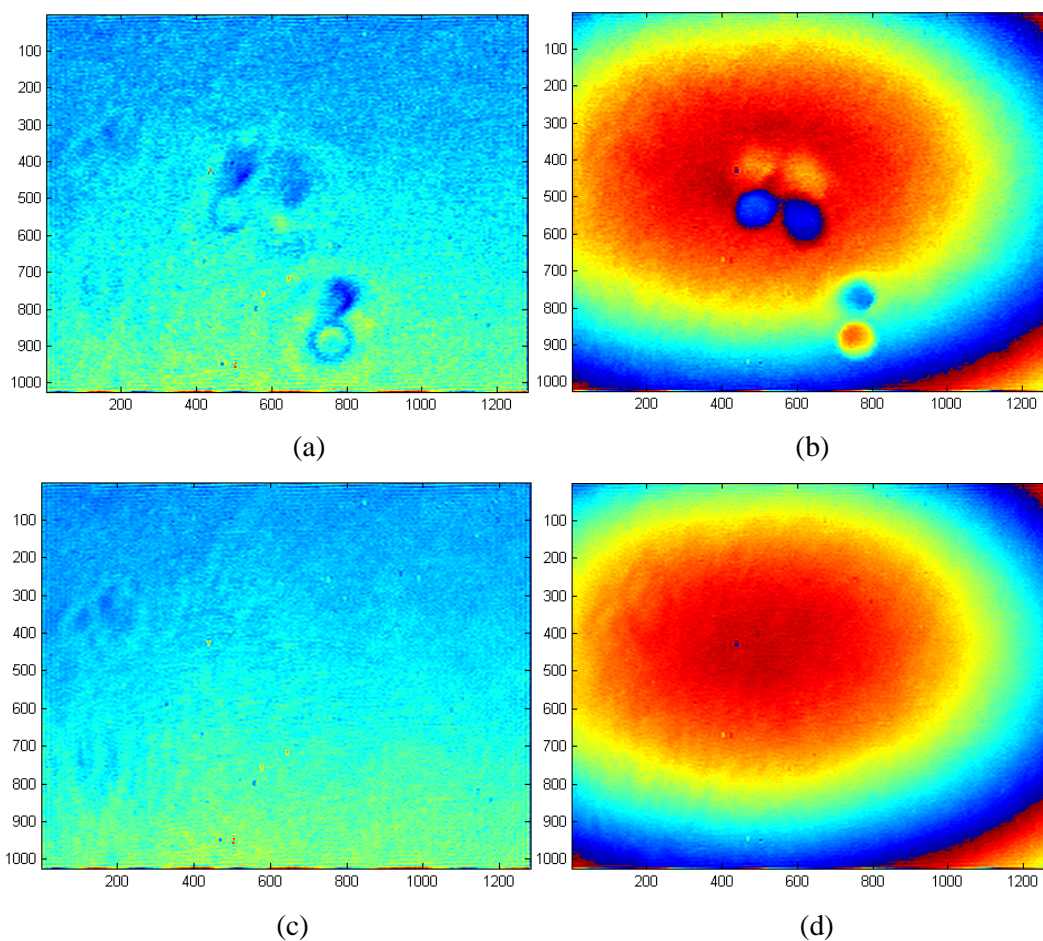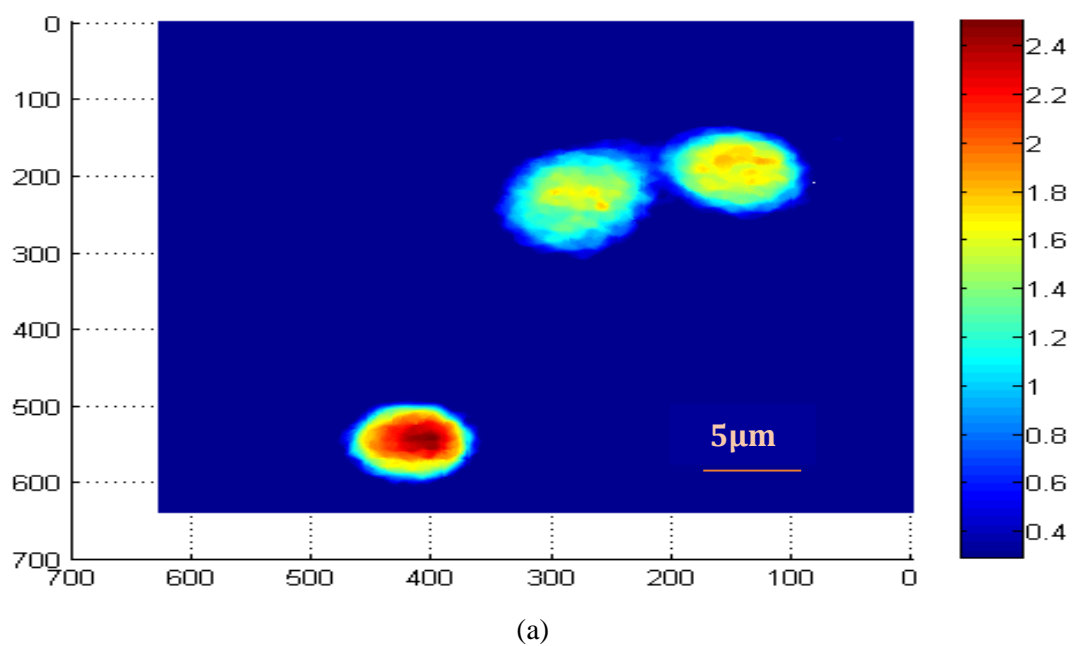
Figure 4-3: (a) Amplitude of yeast cell hologram(b) Phase map of yeast cell hologram (c) Amplitude of background hologram   (d) Phase of the background hologram
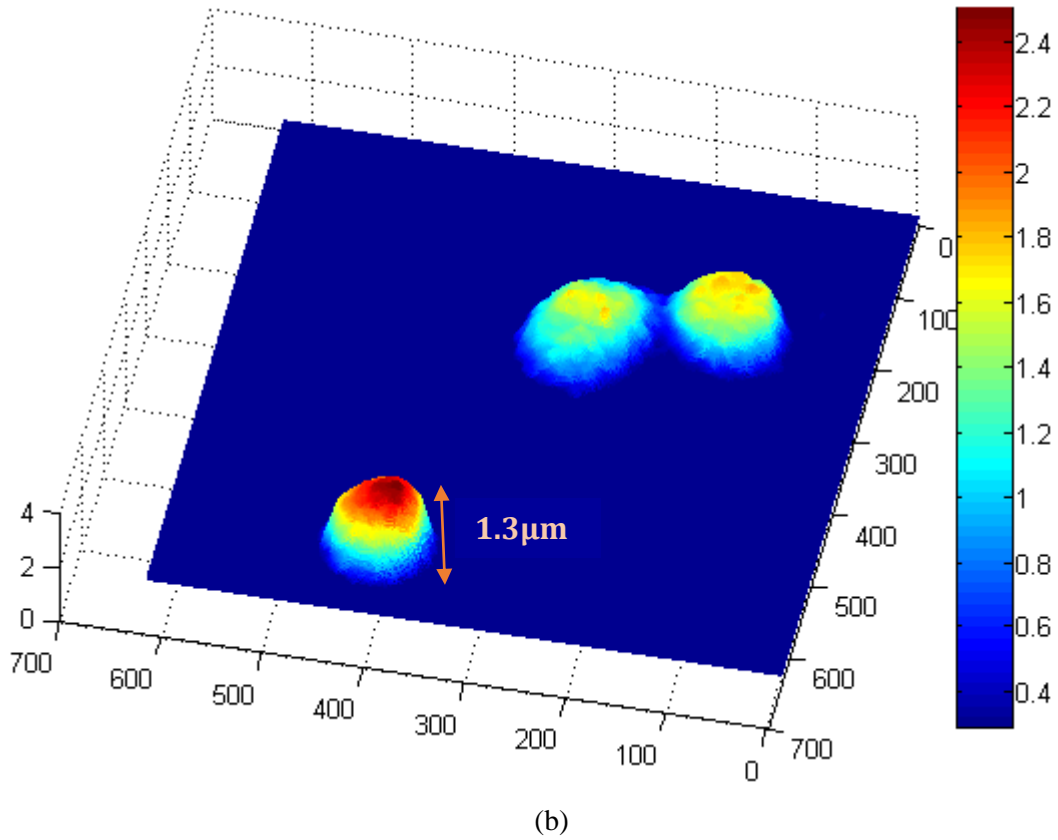

(a)

(b)

Figure 4-4: (a) 2D Phase map of yeast cells (b) 3D Phase map of yeast cells

We have also recorded a video showing the dynamics of yeast cells. We have calculated the thickness of the yeast cell using the Equation (4.1).

$$h(x, y) = \frac{\Delta\phi(x, y)\lambda}{2\pi\Delta\eta} \qquad (4.1) \qquad \text{where}$$

$h(x, y)$ is the local thickness of the yeast cell, $\Delta\phi(x, y)$ is the local phase shift introduced by the specimen, λ is the mean wavelength of the illumination source which is 532nm and $\Delta\eta$ is the refractive index difference between the specimen and medium. Refractive index of yeast cell is 1.51 and refractive index of YPD medium surrounding yeast is 1.339. So the thickness of the yeast cell is calculated to be 1.3μm.

We have also recorded the DPM images for sperm cells and reconstructed phase by using the same algorithm. Sperm cells were fixed by Formalin and resuspended in PBS. Figure 4-5 shows the recorded hologram and reconstructed phase map of sperm cell. Refractive index of sperm cell is 1.53 and of PBS medium is 1.334. So, by using Eq. (4.1), we calculated the thickness of sperm cell to be 773nm.

(a)

0.773μm
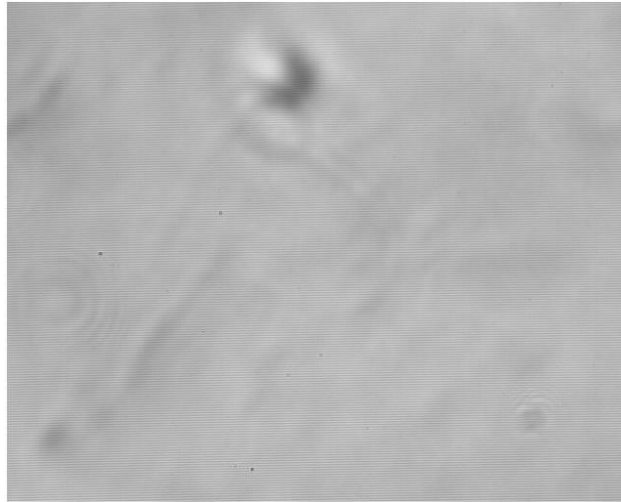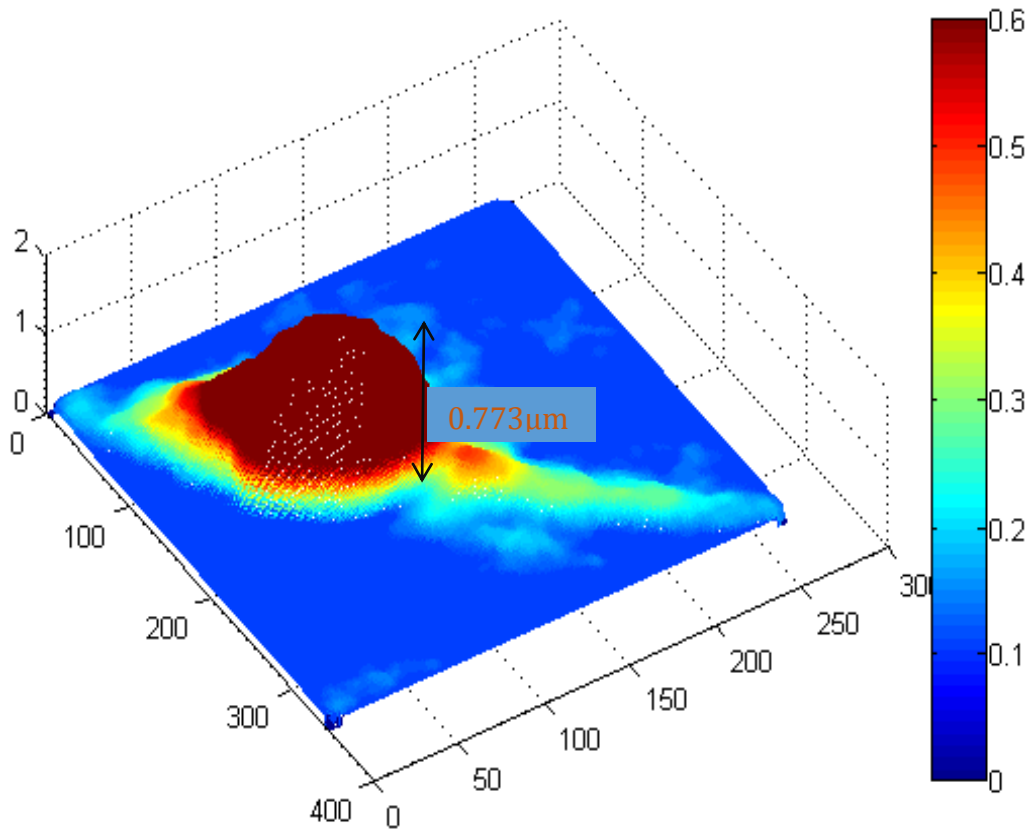
(b)

Figure 4-5: (a) Hologram of sperm cell   (b) Reconstructed phase map

Chapter 5

Conclusion and future work

White light diffraction phase microscopy set up has been developed. Holograms of yeast cells and sperm cells have been recorded. Fast phase reconstruction algorithm has been used for retrieving quantitative phase maps of yeast cells and sperm cells. We have calculated the thickness of these specimen to nanometric resolutions. Main advantages of this technique are temporal and spatial phase sensitivity due to speckle free images. In future we would work on improving the spatial resolutions. We would try to combine multimodalities for improvement. There is a possibility of a tomographic approach so that we can image subcellular structures.

References

1.   Geva, T., *Magnetic resonance imaging: historical perspective.* Journal of Cardiovascular Magnetic Resonance, 2006. **8**(4): p. 573-580.

2.   Shung, K.K., *Diagnostic ultrasound: Past, present, and future.* Journal of Medical and Biological Engineering, 2011. **31**(6): p. 371-374.

3.   Tai, Y. and P. Piccini, *Applications of positron emission tomography (PET) in neurology.* Journal of Neurology, Neurosurgery & Psychiatry, 2004. **75**(5): p. 669-676.

4.   Kitson, S.L., et al., *Clinical applications of positron emission tomography (PET) imaging in medicine: oncology, brain diseases and cardiology.* Current Radiopharmaceuticals, 2009. **2**(4): p. 224-253.

5.   Rydberg, J., et al., *Multisection CT: Scanning Techniques and Clinical Applications 1.* Radiographics, 2000. **20**(6): p. 1787-1806.

6.   Cammoun, D., K.A. Davis, and W.R. Hendee, *Clinical applications of magnetic resonance imaging—current status.* Western Journal of Medicine, 1985. **143**(6): p. 793.

7.   Massoud, T.F. and S.S. Gambhir, *Molecular imaging in living subjects: seeing fundamental biological processes in a new light.* Genes & development, 2003. **17**(5): p. 545-580.

8.   Bilyy, O.I., et al. *Rapid detection of bacterial cells by light scattering method.* in *Biomedical Optics (BiOS) 2008.* 2008. International Society for Optics and Photonics.

9.   "James Hillier". Inventor of the Week: Archive. 2003-05-01, R.-.-.

10.   Francis, L.W., et al., *Atomic force microscopy comes of age.* Biology of the Cell, 2010. **102**(2): p. 133-143.

11.   Erin E. Wilson and Michael W. Davidson – National High Magnetic Field Laboratory, E.P.D.D., The Florida State University.

12.   www.olympusmicro.com

13.   www.nobelprize.org

14.   Petty, H.R., Fluorescence microscopy: established and emerging methods, experimental strategies, and applications in immunology. Microscopy research and technique, 2007. 70(8): p. 687-709.

15.   Abbe, E.B.z.T.d.M.u.d.m.W.A.f.m.A., 9, 431.

16.   Zernike, F.b.P.c., a new method for the microscopic observation of trans¬parent objects, Part 1. Physica, 9, 686–698.

17.   Zernike, F.a.P.c., a new method for the microscopic observation of trans¬parent objects, Part 2. Physica, 9, 974–986.

18.   Gabor, D.A.n.m.p.N., 161, 777.

19.   G. Popescu, Q.P.I.o.C.a.T.M.-H., 2011).

20.   Cuche, E., F. Bevilacqua, and C. Depeursinge, Digital holography for quantitative phase-contrast imaging. Optics letters, 1999. 24(5): p. 291-293.

21.   Ikeda, T., et al., Hilbert phase microscopy for investigating fast dynamics in transparent systems. Optics letters, 2005. 30(10): p. 1165-1167.

22.   Hogenboom, D.O., DiMarzio, C. A., Gaudette, T. J., Devaney, A. J., & Lindberg, S. C. (1998). Threedimensional images generated by quadrature interferometry. Optics Letters, 23, 783–785.

23.   Popescu, G., et al., Fourier phase microscopy for investigation of biological structures and dynamics. Optics letters, 2004. 29(21): p. 2503-2505.

24.   G. Popescu, T.I., R. R. Dasari, and M. S. Feld, Opt. Lett. 31, 775 (2006).

25.   Y. K. Park, G.P., K. Badizadegan, R. R. Dasari, and M. S. Feld, Opt. Express 14, 8263 (2006).

26.   Park, Y., Diez-Silva, M., Popescu, G., Lykotrafitis, G., Choi, W., Feld, M. S., et al. (2008). Refractive index maps and membrane dynamics of human red blood cells parasitized and by Plasmodium falciparum. Proceedings of the National Academy of Sciences of the United States of America, 13730–13735.

27.   Wang, Z., et al., *Spatial light interference microscopy (SLIM).* Optics express, 2011. **19**(2): p. 1016-1026.

28.   Ding, H.a.G.P., Instantaneous spatial light interference microscopy. Optics express, 2010. 18(2): p. 1569-1575.

29.   Petruccelli, J.C., L. Tian, and G. Barbastathis, *The transport of intensity equation for optical path length recovery using partially coherent illumination.* Optics express, 2013. **21**(12): p. 14430-14441.

30.   F. Zernike, P.c., a new method for the microscopic observation of transparent objects, Part 2," Physica 9, 974–986 (1942).

31.   J. W. Goodman and R. W. Lawrence, D.i.f.f.e.d.h., " Appl. Phys. Lett. 11, 77–79 (1967).

32.   M. Takeda, H.I., and S. Kobayashi, "Fourier-transform method of fringepattern, J.O. analysis for computer-based topography and interferometry, and Soc. Am. 72.

33.   K. J. Gåsvik, O.M.W., 2002).

34.   Bhaduri, B., et al., *Diffraction phase microscopy: principles and applications in materials and life sciences.* Advances in Optics and Photonics, 2014. **6**(1): p. 57-119.

35.   E. Abbe, B.z.T.d.M.u.d.m. and A.M.A. Wahrnehmung, 413–468 (1873).

36.   B. E. A. Saleh and M. C. Teich, F.o.P.W., 2013).

37.   Bhaduri, B., et al., *Diffraction phase microscopy with white light.* Optics letters, 2012. **37**(6): p. 1094-1096.

38.   Edwards, C., et al., *Effects of spatial coherence in diffraction phase microscopy.* Optics express, 2014. **22**(5): p. 5133-5146.

39.   Nguyen, T.H., et al., *Quantitative phase imaging with partially coherent illumination.* Optics letters, 2014. **39**(19): p. 5511-5514.

40.   Ikeda, T., et al., *Hilbert phase microscopy for investigating fast dynamics in transparent systems.* Optics letters, 2005. **30**(10): p. 1165-1167.

41.   Pham, H.V., et al., *Fast phase reconstruction in white light diffraction phase microscopy.* Applied optics, 2013. **52**(1): p. A97-A101.